Shifting media induced super-resolution imaging

2015 J. Opt. 17 025606

(http://iopscience.iop.org/2040-8986/17/2/025606)

IOP Publishing Journal of Optics
J. Opt. 17 (2015) 025606 (8pp) doi:10.1088/2040-8978/17/2/025606

Shifting media induced super-resolution imaging

Yong Du, XiaoFei Zang, Cheng Shi, XueBin Ji and YiMing Zhu

Shanghai Key Lab of Modern Optical System and Engineering Research Center of Optical Instrument and System, Ministry of Education, University of Shanghai for Science and Technology, Shanghai 200093, People's Republic of China

E-mail: xfzang@usst.edu.cn and ymzhu@usst.edu.cn

Received 6 October 2014, revised 26 November 2014
Accepted for publication 27 November 2014
Published 14 January 2015

Abstract

In this paper, we propose a novel method to achieve super-resolution imaging by utilizing shifting media based on the transformation optics theory. According to the effective medium theory, the homogenous but anisotropic shifting media can be simply replaced by only two kinds of homogenous and isotropic materials in an alternating layered structure. In addition, another scheme of the symmetrical trapezoidal shifting media shells with layered isotropic materials is proposed to realize the super-resolution imaging. Finite element simulations have been performed to prove these ideas.

Keywords: transformation optics, metamaterials, super-resolution imaging

(Some figures may appear in colour only in the online journal)

1. Introduction

In the past few years, transformation optics (TO) [1, 2] has attracted great attention. Based on TO, the most exciting and fascinating device is the invisibility cloak [3–15]. According to the coordinate transformation and the form invariance property of Maxwell's equations, a free space can be compressed into a shell thus forming a hidden region, in which an object cannot be detected, leading to an invisible cloak. In addition, TO was also applied into other novel devices: a waveguide connector [16, 17], which can tunnel the electromagnetic wave along arbitrary directions; an illusion system [18], which is able to make an object appear like another one; the super-absorber [19], which induces strong absorption by amplifying the evanescent tail of high-order cylindrical waves; and the super-scatterer [20], which can make an object seem bigger than its original size by enhancing the wave scattering cross section; and so on.

In this paper, TO-based shifting media are extended into super-resolution imaging. As is well known, the resolution of conventional lenses are constrained by the fundamental 'diffraction limit', which is mainly caused by the absence of the evanescent waves carrying the high-spatial-frequency information in the far-field [21]. To overcome this bottleneck, J. B. Pendry has proposed a perfect lens consisting of double negative-index material to achieve perfect imaging by enhancing the near-field evanescent waves [22]. Subsequently, simplified perfect lenses, such as silver-superlens [23] and SiC-superlens [24], have been theoretically designed and practically realized. However, these superlenses are also only capable of projecting sub-diffraction-limited images in the near field, because the evanescent waves will still decay exponentially away from such lenses. Recently, the far-field superlens (FSL) [25, 26] and the hyperlens [27–32] have made a lot of progress in far-field imaging. The FSL consists of a silver slab and periodic sub-wavelength grating, in which the evanescent waves are enhanced in the silver slab. Then the enhanced evanescent waves are converted into propagating waves in periodic grating, resulting in far-field, super-resolution imaging. Different from the FSL, the hyperlens is composed of anisotropic and multilayer metamaterials in a curved geometry, which can generate hyperbolic or eccentric elliptic dispersions to support the propagation of high wavevector waves. A special hyperlens, or metalens, created by combining a metamatarial slab and a phase-compensation structure, provides not only the high-resolution capabilities, but also the Fourier transform function [32]. In fact, based on TO, these analogous superlenses and hyperlenses can also be of theoretical or practical design [33–36]. For example, Weixiang Jiang *et al* manufactured an adielectric

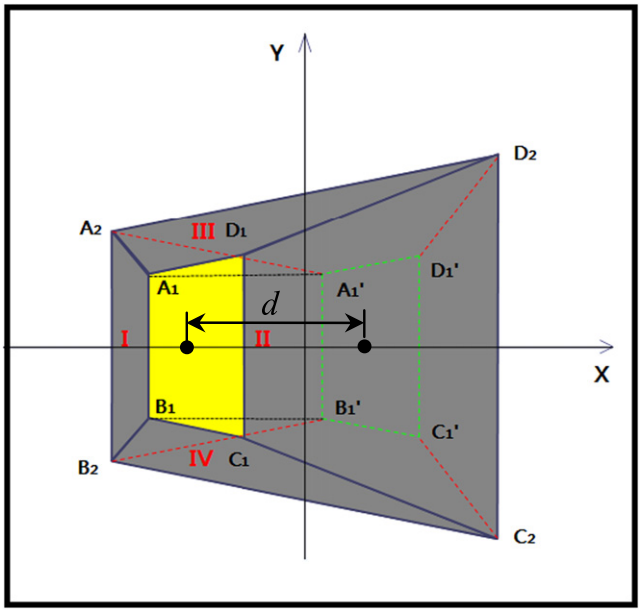

Figure 1. Schematic of shifting media. The yellow region is physical space, the region surrounded by the green dummy line is virtual space and the gray regions are shifting media. Region $A_1B_1C_1D_1$ (physical space) is shifted into region $A_1'B_1'C_1'D_1'$ (virtual space) by using shifting media.

metamaterial magnifying lens, which utilizes metamaterial with a gradient refractive index to realize sub-diffraction-limited resolution [33]. Wei Wang *et al* proposed a far-field planar hyperlens, whose imaging magnification is realized by using multilayer metamaterials [34]. In addition, a super-resolution imaging transfer with a vertex-like metamaterial was reported by Huiyuan Dong *et al* [35].

Here, we propose another new kind of method to realize super-resolution imaging in the far field by using shifting media based on TO theory. Different from the previous superlenses engineered by the left-hand materials with negative refraction index and hyperlenses based on anisotropic metamaterials, this shifting media can be designed by homogeneous and isotropic materials with positive permittivity and permeability, i.e., positive index of refraction based on the effective medium theory [37, 38].

2. Theory

Figure 1 schematically depicts a shifting media device in a Cartesian coordinate system, where a small trapezoidal object (yellow region) is coated with a trapezoidal shifting media shell (gray region). In this situation, the region $A_1'B_1'B_2\,A_2$ is folded into $A_1\,B_1\,B_2\,A_2$ (region I). Meanwhile, $D_1'C_1'C_2\,D_2$, $A_1'D_1'D_2\,A_2$, and $B_1'C_1'C_2\,B_2$ are mapped into $D_1\,C_1\,C_2\,D_2$ (region II), $A_1\,D_1\,D_2\,A_2$ (region III) and $B_1C_1C_2B_2$ (region IV), respectively. Therefore, the physical space (region $A_1B_1C_1D_1$) covered with shifting media will be shifted to the virtual region of $A_1'B_1'C_1'D_1'$. Accordingly, if we put a point-source in the region of $A_1B_1C_1D_1$, the corresponding position will be shifted into the region of $A_1'B_1'C_1'D_1'$ with a shifting distance of d. The coordinate of each point in figure 1 is A_1 $(-a_{11}, h_{11})$, B_1 $(-a_{11}, -h_{11})$, C_1 $(-a_{12}, h_{12})$, D_1 $(-a_{12}, h_{12})$, A_2 $(-a_{21}, h_{21})$, B_2 $(-a_{21}, -h_{21})$, C_2 $(a_{21}, -h_{22})$, D_2 (a_{21}, h_{22}). According to the theory of transformation optics, the coordinate transformation between the virtual space and the physical space can be expressed as:

In region I:

$$\begin{aligned} x' &= m_1 x + \frac{d\left(a_{21} - 2a_{11} + d\right)}{a_{21} - a_{11} + d} \\ y' &= y \\ z' &= z \end{aligned} \tag{1}$$

where $m_1 = \frac{a_{21} - a_{11}}{a_{21} - a_{11} + d}$

In region II:

$$\begin{aligned} x' &= m_2 x + \frac{d\left(a_{21} + 2a_{12} - d\right)}{a_{21} + a_{12} - d} \\ y' &= y \\ z' &= z \end{aligned} \tag{2}$$

where $m_2 = \frac{a_{21} + a_{12}}{a_{21} + a_{12} - d}$

In region III and IV:

$$\begin{aligned} x' &= m_3 x \mp m_4 y + m_5 \\ y' &= y \\ z' &= z \end{aligned} \tag{3}$$

where '–' and '+' correspond to region III and IV, respectively, and

$$m_3 = \frac{\left(h_{22} - h_{21}\right)\left(a_{12} + a_{21}\right) + 2a_{21}\left(h_{12} - h_{22}\right)}{\left(h_{22} - h_{21}\right)\left(a_{21} + a_{12} - d\right) + 2a_{21}\left(h_{12} - h_{22}\right)}$$

$$m_4 = \frac{2a_{21}d}{\left(h_{22} - h_{21}\right)\left(a_{21} + a_{12} - d\right) + 2a_{21}\left(h_{12} - h_{22}\right)}$$

$$m_5 = \frac{a_{21}d\left(h_{22} + h_{21}\right)}{\left(h_{22} - h_{21}\right)\left(a_{21} + a_{12} - d\right) + 2a_{21}\left(h_{12} - h_{22}\right)}$$

The corresponding permittivity and permeability tensors in regions I–IV are given as follows: In region I:

$$\varepsilon = \mu = \begin{bmatrix} m_1 & 0 & 0 \\ 0 & 1/m_1 & 0 \\ 0 & 0 & 1/m_1 \end{bmatrix} \tag{4}$$

In region II:

$$\varepsilon = \mu = \begin{bmatrix} m_2 & 0 & 0 \\ 0 & 1/m_2 & 0 \\ 0 & 0 & 1/m_2 \end{bmatrix} \tag{5}$$

In regions III and IV:

$$\varepsilon = \mu = \begin{bmatrix} \left(m_3^2 + m_4^2\right)/m_3 & \mp m_4/m_3 & 0 \\ \mp m_4/m_3 & 1/m_3 & 0 \\ 0 & 0 & 1/m_3 \end{bmatrix} \tag{6}$$

where '–' and '+' are correspond to region III and IV, respectively.

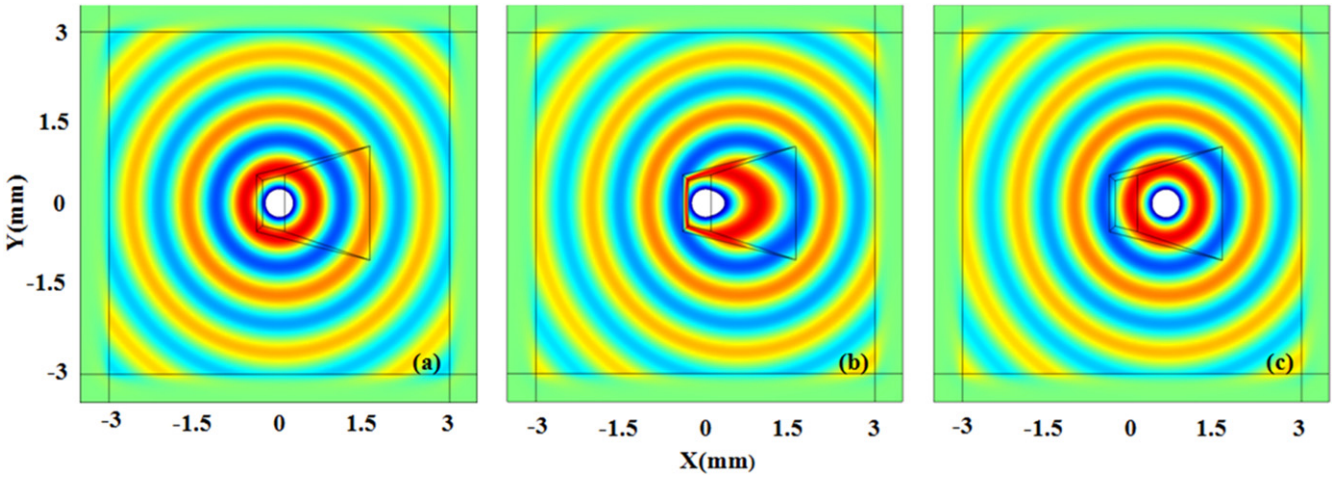

Figure 2. The electric field distribution for a point-source with wavelength of 1 mm located at (0, 0) (**a**) without shifting media and (**b**) with shifting media (d = 0.6 mm). (**c**) The electric field distribution for a point-source located at (0.6 mm, 0) without shifting media.

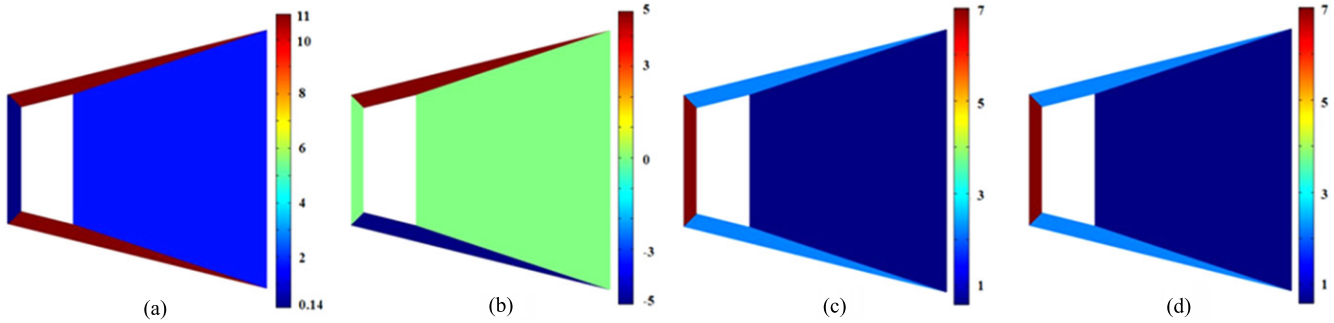

Figure 3. Permittivity and permeability tensor parameters for the shifting media: (**a**) μ_{xx}, (**b**) $\mu_{xy} = \mu_{yx}$, (**c**) μ_{yy} and (**d**) ε_{zz}.

It should be noted that the shifting media is homogenous but anisotropic.

3. Numerical simulation and discussion

First, we performed numerical simulation by using the finite element method (FEM) to demonstrate the shifting effect of the transformation media, as shown in figure 2. Here, we define $a_{11} = 0.9$ mm, $a_{12} = 0.5$ mm, $a_{21} = 1$ mm, $h_{11} = 0.4$ mm, $h_{12} = 0.5$ mm, $h_{21} = 0.5$ mm, $h_{22} = 1$ mm and $d = 0.6$ mm. Figures 2(a) and (c) depict the electric field distributions of a point-source (wavelength is 1 mm) located at (0, 0) and (0.6 mm, 0) in free space (air), respectively. The permittivity and permeability of the trapezoidal region in figures 2(a) and (c) are $\varepsilon = \mu = 1$. Figure 2(b) shows the field distribution of a point-source at (0, 0) and covered with shifting media (shifting distance is d = 0.6 mm). Comparing figures 2(b) and (c), it can be seen that both have the same field distribution outside the transformation region. Hence, the point-source located at (0, 0) in figure 2(b) is shifted to the position (0.6 mm, 0) due to the shifting media. The corresponding material parameters of the shifting media shell are shown in figure 3, in which we can see the material of the shifting media is anisotropic but homogeneous.

Now, we study the super-resolution imaging based on the shifting effect of the shifting media. Figure 4(a) illustrates the electric field distribution of two separated point-sources in free space with a separation distance of $\lambda/4$ ($\lambda = 1$ mm). In this case, two separated point-sources are very difficult to distinguish, because they resemble a single source in the far-field region due to the 'diffraction limit' [the green line in figure 4(d)]. To distinguish the two separate point-sources, we have to enlarge their separation distance larger than a half wavelength of incident electromagnetic wave according to the Abble diffraction limit theory. In figure 4(c), we depict the electricfield distribution of the two separated point-sources located in free space with a separation distance of $\lambda/4 + d$ ($d = 0.6^*\lambda$, and $\lambda/4 + d > \lambda/2$). Remarkably different from the case of figure 4(a), these two separated point-sources in figure 4(c) appear as strong or weak electric field distribution, which means that these point-sources in figure 4(c) is distinguished, and the strong or weak electric field distribution is due to the coherent effect between these two distinguished sources. In figure 4(b), we show the electric field distribution of two separated point-sources (the separation distance is $\lambda/4$), for the right point-source coating with the shifting media. Both figures 4(b) and (c) show identical features outside the transformation region, implying that these two point-sources in figure 4(b) can also be distinguished, although the separation distance between them is less than $\lambda/2$. Meanwhile, figure 4(d) represents the

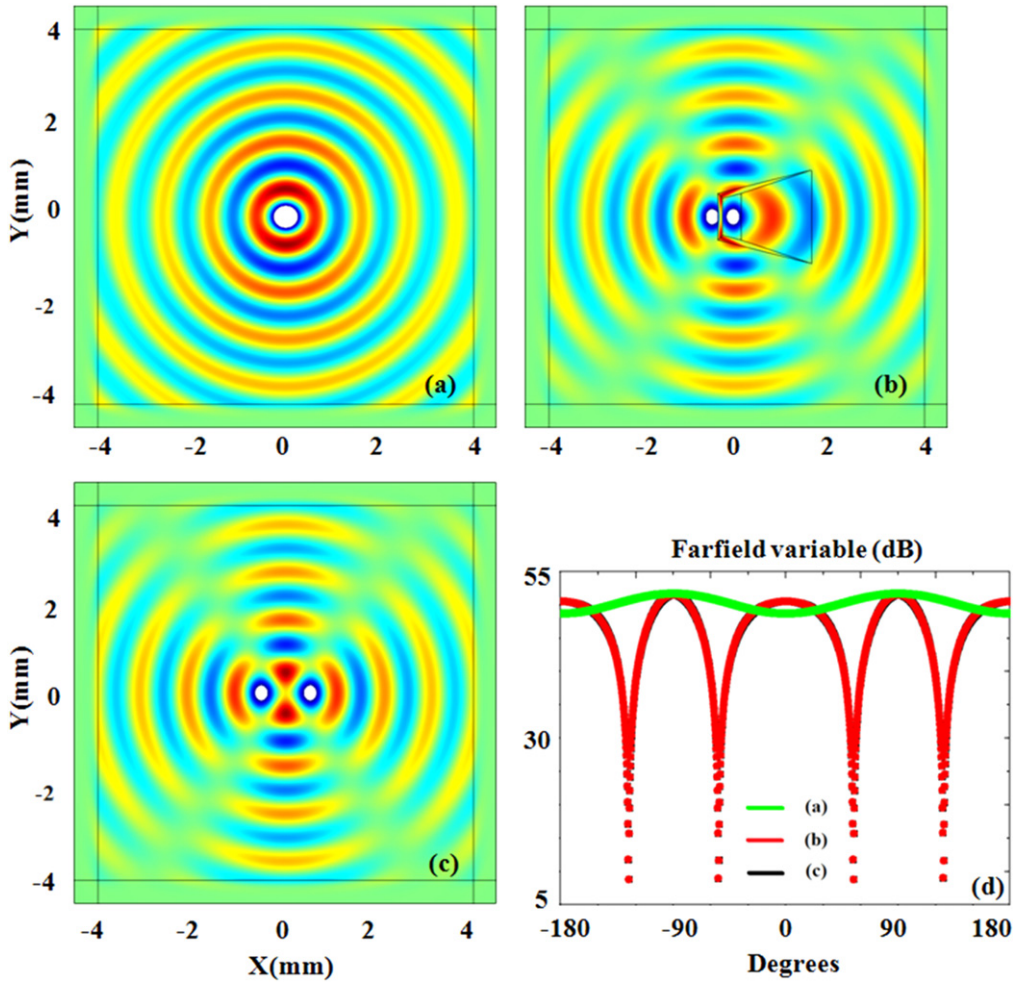

Figure 4. (a) The electric-field distribution of two separated point-sources with a separation distance of $\lambda/4$ in free space. (b) The electric field distribution of two separated point-sources (separation distance is $\lambda/4$) when the right point-source coated by the shifting media with the shifting distance d = 0.6 mm. (c) The electric field distribution of two separated point-sources with a separation distance of $\lambda/4 + d$ ($\lambda/4 + d > \lambda/2$) in free space. (d) The corresponding far-field features at r = 11 mm of (a) (green line), (b) (red line) and (c) (black line).

corresponding far-field radiation of figures 4(a)–(c) at r = 11 mm (r > 10*λ, and λ = 1 mm, where r is the distance from (0, 0) to an arbitrary point in the simulation region). It should be noted that the green curve depicting the far-field features of figure 4(a) just like a straight line (two separated sources are nearly overlapped with each other, and they cannot be distinguished), while the far-field features of figure 4(b) (red curve) are the same as that of figure 4(c) (black curve), and both of them have four peaks (due to the coherent effect) at 0°, 90°, 180° and −90°, respectively. So the far-field results also certify that based on shifting media, two separated point-sources with a separation distance of less than $\lambda/2$ can be easily distinguished from each other.

Although the feasibility of the shifting media shell consisting of homogenous and anisotropic materials on the field of super-resolution imaging is verified in figure 3, it is difficult to design the shifting media shell by anisotropic materials, and it is very hard to be found in nature and fabricated. Based on the effective medium theory [30, 31], the homogenous but anisotropic shifting media shown above can simply be replaced by an alternating layered structure of homogeneous and isotropic materials, as shown in figure 5. According to reference [30], the parameters of the layered isotropic materials (medium-A and medium-B) in each region can be expressed as:

$$\mu_i^{A,B} = \alpha_i^x \pm \sqrt{(\alpha_i^x)^2 - \alpha_i^x \alpha_i^y}$$

where

$$\alpha_i^{x,y} = \left[\mu_i^{xx} + \mu_i^{yy} \pm \sqrt{(\mu_i^{xx} - \mu_i^{yy})^2 + (2\mu_i^{xy})^2}\right] \Big/ 2,$$

$\varepsilon_i = \alpha_i^z = \mu_i^{zz} (i = I, II, III \text{ and } IV)$, and the angle between the layer and $\boldsymbol{x}$-axis can be determined by

$$\tan(2\theta_i) = 2\mu_i^{xy} / (\mu_i^{xx} - \mu_i^{yy}).$$

Here, we set M = 40 (the number of layers) for all the regions (regions I, II, III and IV), and the effective isotropic parameters can be expressed as $\mu_I^A = 13.9282$, $\mu_I^B = 0.0718$, $\varepsilon_I = 7$, $\mu_{II}^A = 3.0001$, $\mu_{II}^B = 0.3333$, $\varepsilon_{II} = 0.6$ and $\mu_{III}^A = \mu_{IV}^A = 26.063$, $\mu_{III}^B = \mu_{IV}^B = 0.0384$, $\varepsilon_{III} = \varepsilon_{IV} = 2.2$. Figure 5(a) shows the electric-field distribution of two separated point-sources in free space with a separation distance of $\lambda/4$, in which two separated point-sources are very difficult to

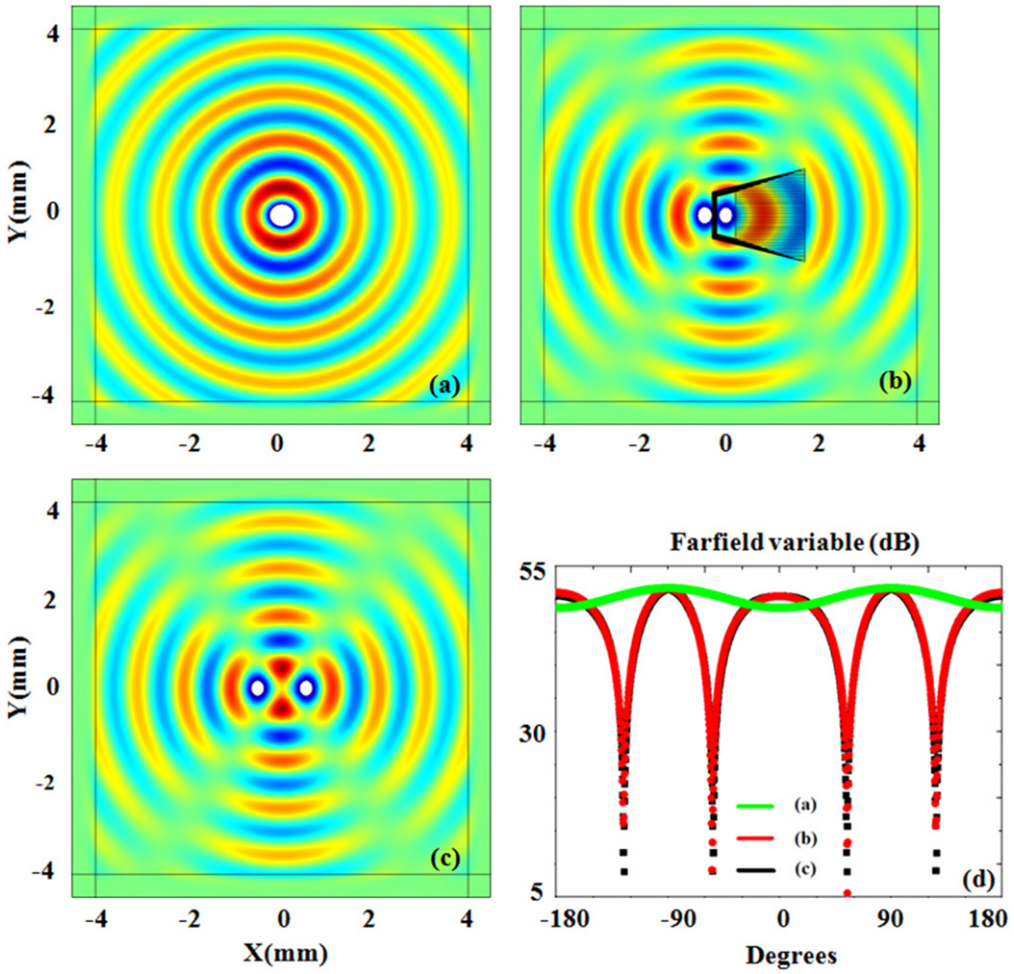

Figure 5. (a) The electric field distribution of two separated point-sources with a separation distance of $\lambda/4$ ($\lambda = 1$ mm) in free space. (b) The electric field distribution of two separated point-sources (separation distance is $\lambda/4$) when the right point-sources coated by the layered shifting media shell with $\theta_{\mathrm{I}} = 90°$, $\theta_{\mathrm{II}} = 0°$, $\theta_{\mathrm{III}} = 23.8631°$, $\theta_{\mathrm{IV}} = -23.8631°$ and shifting distance d = 0.6 mm. (c) The electric field distribution of two separated point-sources with a distance of $\lambda/4 + \mathrm{d}$ ($\lambda/4 + \mathrm{d} > \lambda/2$) in free space. (d) The corresponding far-field features at r = 11 mm of (a) green line, (b) red line and (c) black line.

distinguish because the field distribution is homogeneous. When one of these point-sources is embedded in the shifting media shell composed of layered isotropic transformation media, these two separated point-sources with a separation distance of $\lambda/4$ appear with a strong or weak electric-field distribution [figure 5(b)] and become the same as the field distribution of two separated point-sources with a separation distance of $\lambda/4 + \mathrm{d}$ ($\lambda/4 + \mathrm{d} > \lambda/2$) in free space [figure 5(c)]. This demonstrates that the two undistinguished point-sources can be easily distinguished due to the layered shifting media. In order to verify the far-field effect of the isotropic layered shifting media shell, we also simulate the corresponding radiation patterns, as shown in figure 5(d). Comparing these curves, the far-field features of figure 4(b) (red curve) are identical to that of figure 4(c) (black curve) indicating that by using the shifting media of layered isotropic materials, two separated point-sources with a separation distance of less than the 'differential limit' can also be distinguished.

Figure 6 shows another method to realize super-resolution imaging by using a symmetrical layered shifting media. Figure 6(a) depicts a homogeneous electric field distribution of two separated point-sources in free space with an undistinguished distance of $\lambda/5$. Figure 6(b) shows the electric field distribution of two separated point-sources with separation distance of $\lambda/5$ ($\lambda = 1$ mm) surrounded by symmetrical trapezoidal shifting media shells with alternating layered isotropic materials, respectively. Figure 6(c) illustrates the electric field distribution of two separated point-sources with a separation distance of $\lambda/5 + 2{*}\mathrm{d}$ ($\mathrm{d} = 0.3{*}\lambda$, and $\lambda/5 + 2{*}\mathrm{d} > \lambda/2$) in the free space. Comparing figures 6(b) and (c), we can find that they both have the same strong or weak electric field distribution [also see the very similar far-field radiation patterns with 4 peaks at 0°, 90°, 180° and −90°, respectively in figure 6(d)], which demonstrates that two undistinguished point-sources can also be easily distinguished by utilizing the symmetrical layered shifting media. Hence, the proposed structure of the symmetrical trapezoidal shifting media shells with homogeneous and isotropic materials is also verified to realize the super-resolution imaging.

The presented shifting media can be realized by constructing appropriate periodical *L–C* transmission line network. Based on the transmission line network theory and

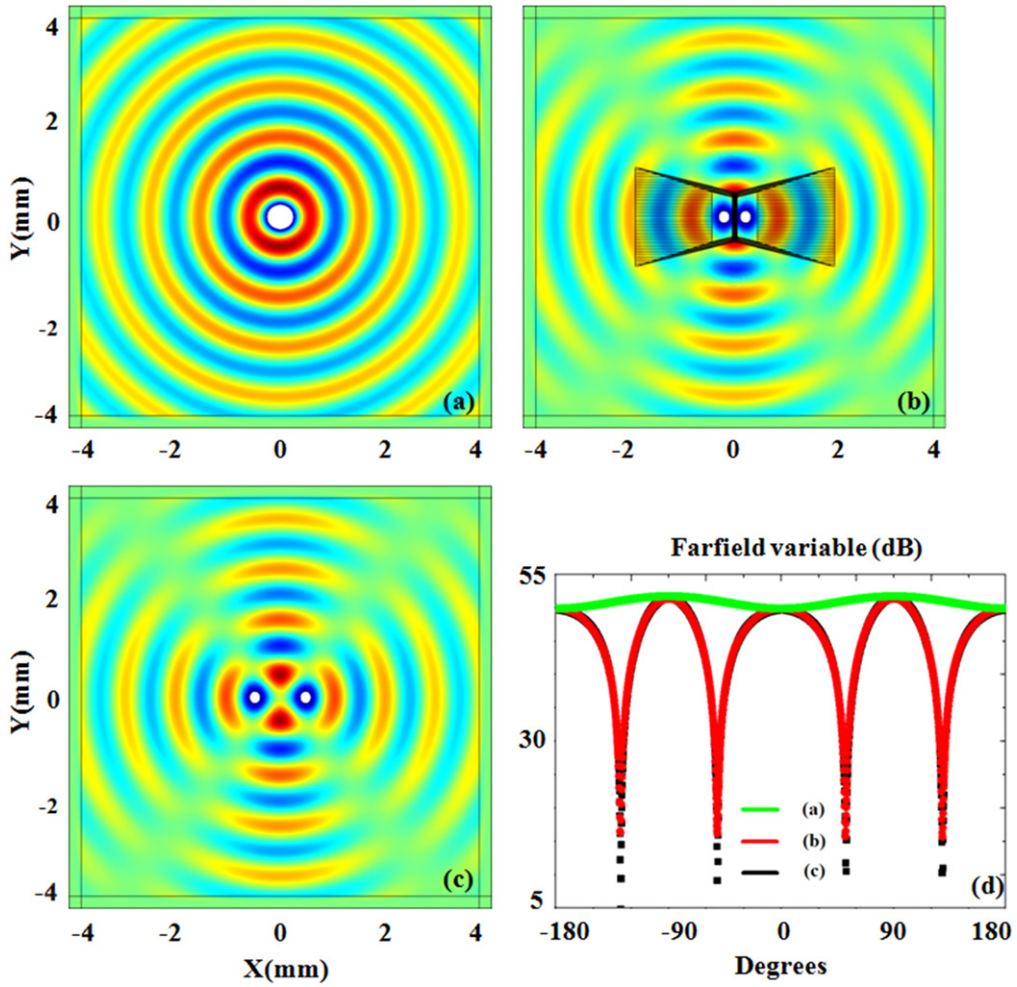

Figure 6. (a) The electric field distribution of two separated point-sources with a separation distance of **λ/5** in free space. (b) The electric field distribution of two separated point-sources (separation distance is λ/5) coated by two layered shifting media shells, respectively, with $\theta_I = 90°$, $\theta_{II} = 0°$, $\theta_{III} = 29.5188°$, $\theta_{IV} = -29.5188°$ and the shifting distance d = 0.3 mm. (c) The electric field distribution of two separated point-sources with separation distance of λ/5 + 2*d (λ/5 + 2*d > λ/2) in free space. (d) The corresponding far-field features at r = 11 mm of (a) blue line, (b) red line and (c) black line.

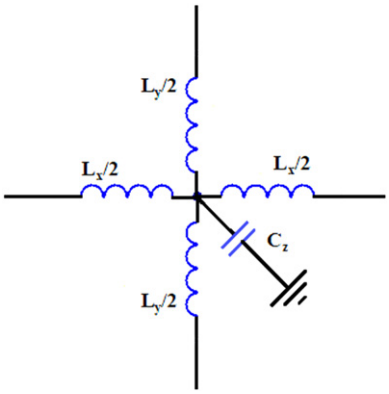

Figure 7. Unit cell of *L–C* transmission line network, where L_x and L_y are the inductances and C_z is the capacitance of the unit cell.

electromagnetic theory, the series inductors and shunt capacitor in figure 7 can act as an isotropic medium with positive parameters for $L_x = L_y$, which have been applied into many experiments of Refs [39–41]. Here, we can also utilize the method about periodical *L–C* transmission line network to achieve the isotropic materials of the alternating layered shifting media. Figure 7 shows a unit cell of the *L–C* transmission line network to mimic the air region. Based on the long-wavelength limit, the relationship between the effective material parameters and the circuit parameters can be written as:

$$\mu_x = L_y/\Delta$$
$$\mu_y = L_x/\Delta$$
$$\varepsilon_z = C_z/\Delta \quad (7)$$

Where $\Delta = 5$ mm is the unit cell length. The parameters in detail of *L–C* transmission line network are listed in table 1.

Table 1. The unit cell parameters of the ***L–C*** network. (Package size is 0603).

	Air	I	II	III & IV
L_x(nH)	33	470	100	1000
L_y(nH)	33	2.2	11	1.2
C_z(pF)	39	270	22	82

4. Conclusion

In summary, the use of shifting media as another new method to achieve far-field super-resolution imaging, has been theoretically proposed based on TO theory. Unlike hyperlenses and metalenses engineered by anisotropic materials, and superlenses based on left-hand media, an alternating layered structure of homogeneous and isotropic materials with positive permittivity and permeability (i.e. positive index of refraction) can be used to design this shifting media due to the effective medium theory. Both the theory model and numerical simulations demonstrate that this shifting media may open a new perspective for super-resolution imaging.

Acknowledgments

This work is partly supported by the National Program on Key Basic Research Project of China (973 Program, 2014CB339806), Major National Development Project of Scientific Instrument and Equipment (2011YQ150021, 2012YQ14000504, 2012YQ150092), National Natural Science Foundation of China (61138001, 61205094, 61307126), the Key Scientific and Technological Project of Science and Technology Commission of Shanghai Municipality (2014XD140300) (12JC1407100), the Scientific Research Innovation Project of Shanghai Municipal Education Commission (14YZ093), and New Century Excellent Talents from Ministry of Education (NCET-12-1052) and the university young teacher training scheme of Shanghai (ZZSLG13015).

References

[1] Leonhardt U 2006 Optical conformal mapping *Science* **312** 1777–80
[2] Pendry J B, Schuring D and Smith D R 2006 Controlling electromagnetic fields *Science* **312** 1780–2
[3] Schurig D, Mock J J, Justice B J, Cummer S A, Pendry J B, Starr A F and Smith D R 2006 Metamaterial electromagnetic cloak at microwave frequencies *Science* **314** 977–80
[4] Li J and Pendry J B 2008 Hiding under the carpet: a new strategy for cloaking *Phys. Rev. Lett.* **101** 203901
[5] Liu R, Ji C, Mock J J, Chin J Y, Cui T J and Smith D R 2009 Broadband ground-plane cloak *Science* **323** 366–9
[6] Zhou F, Bao Y J, Cao W, Stuart C T, Gu J Q, Zhang W L and Sun C 2011 Hiding a realistic object using a broadband Terahertz invisibility cloak *Sci. Rep.* **1** 78
[7] Ergin T, Stenger N, Brenner P, Pendry J B and Wengener M 2010 Three-dimensional invisibility cloak at optical wavelengths *Science* **328** 337–9
[8] Ma H, Qu S, Xu Z and Wang J F 2009 The open cloak *Appl. Phys. Lett.* **94** 103501
[9] Xi S, Chen H S, Wu B I and Kong J A 2009 One-directional perfect cloak created with homogeneous material *IEEE Microwave and Wireless Components Letters* **19** 131–3
[10] Kwon D H and Werner D H 2008 Two-dimension eccentric electromagnetic cloaks *Appl. Phys. Lett.* **92** 013505
[11] Lai Y, Chen H Y, Zhang Z Q and Chan C T 2009 Complementary media invisibility cloak that cloaks objects at a distance outside the cloaking shell *Phys. Rev. Lett.* **102** 093901
[12] Xu X F, Feng Y J, Yu Z Z, Jiang T and Zhao J 2010 Simplified ground plane invisibility cloak by multilayer dielectrics *Opt. Exp.* **18** 24477
[13] Xu X F, Feng Y J, Xiong S, Fan J L, Zhao J M and Jiang T 2011 Broad band invisibility cloak made of normal dielectric multilayer *Appl. Phys. Lett.* **99** 154104
[14] Ma H F and Cui T J 2010 Three-dimension broadband ground-plane cloak made of metamaterials *Nat. Commun.* **1** 21
[15] Zhang J J, Liu L, Luo Y, Zhang S and Mortensen N A 2011 Homogeneous optical cloak constructed with uniform layered structures *Opt. Exp.* **19** 8625–31
[16] Zhang K, Wu Q, Meng F and Li L W 2010 Arbitrary waveguide connector based on embedded optical transformation *Opt. Exp.* **18** 17273–9
[17] Zhang K, Meng F, Wu Q, Fu J and Li L W 2012 Waveguide connector constructed by normal layered dielectric materials based on embedded optical transformation *EPL* **99** 47008
[18] Lai Y, Ng J, Chen H Y, Han D Z, Xiao J J, Zhang Z Q and Chan C T 2009 Illusion optics: the optical transformation of an object into another object *Phys. Rev. Lett.* **102** 253902
[19] Ng J, Chen H Y and Chan C T 2009 Metamaterial frequency-selective superabsorber *Opt. Lett.* **34** 644–6
[20] Yang T, Chen H Y, Luo X D and Ma H R 2008 Superscatterer: enhancement of scattering with complementary media *Opt. Exp.* **16** 18545–50
[21] Born M and Wolf E 1999 *Principles of Optics* (Cambridge: Cambridge University Press)
[22] Pendry J B 2000 Negative refraction makes a perfect lens *Phys. Rev. Lett.* **85** 3966–9
[23] Fang N, Lee H, Sun C and Zhang X 2005 Sub-diffraction-limited optical imaging with a silver superlens *Science* **308** 534–7
[24] Taubner T, Korobkin D, Urzhumov Y, Shvets G and Hillenbrand R 2006 Near-field microscopy through a SiC superlens *Science* **313** 1595
[25] Xiong Y, Liu Z W, Sun C and Zhang X 2007 Two-dimension imaging by far-field superlens at visible wavelengths *Nano Lett.* **7** 3360–5
[26] Durant S, Liu Z W, Steele J M and Zhang X 2006 Theory of the transmission properties of an optical far-field superlens for imaging beyond the diffraction limit *J. Opt. Soc. Am.* B **23** 2383–92
[27] Jacob Z, Alekseyev L V and Narimanov E 2006 Optical hyperlens: far-field imaging beyond the diffraction limit *Opt. Express* **14** 8247–56
[28] Salandrino A and Engheta N 2006 Far-field subdiffraction optical microscopy using metamaterial crystals: theory and simulations *Phys. Rev.* B **74** 075103
[29] Smolyaninov I I, Huang Y J and Davis C C 2007 Magnifying superlens in the visible frequency range *Science* **315** 1699–701
[30] Liu Z W, Lee H, Xiong Y, Sun C and Zhangion X 2007 Far-field optical hyperlens magnifying sub-diffract-limited objects *Science* **315** 1686
[31] Rho J, Ye Z L, Xiong Y, Yin X B, Liu Z W, Choi H, Bartal G and Zhang X 2010 Spherical hyperlens for two-dimensional sub-diffractional imaging at visible frequencies *Nat. Commun.* **1** 143
[32] Lu D and Liu Z W 2012 Hyperlenses and metalenses for far-field super-resolution imaging *Nat. Commun.* **3** 1205
[33] Jiang W X, Qiu C W, Han T C, Cheng Q, Ma H F, Zhang S and Cui T J 2013 Broadband all-dielectric magnifying lens for far-field high-resolution imaging *Adv. Mater.* **25** 6963–8

[34] Wang W, Xing H, Fang L, Liu Y, Ma J, Lin L, Wang C and Luo X 2008 Far-field imaging device: planar hyperlens with magnification using multi-layer metamaterial *Opt. Express.* **16** 21142

[35] Dong H Y, Wang J, Fung K H and Cui T J 2013 Super-resolution image transfer by a vortex-like metamaterial *Opt. Exp.* **21** 9407

[36] Tsang M and Psaltis D 2008 Magnifying perfect lens and superlens design by coordination transformation *Phys. Rev.* B **77** 035122

[37] Hang T C, Qiu C W, Dong J W, Tang X H and Zouhdi S 2011 Homogeneous and isotropic bends to tunnel waves through multiple different/equal waveguides along arbitrary directions *Opt. Exp.* **19** 13020–30

[38] Qiu C W, Hu L, Xu X F and Feng Y J 2009 Spherical cloaking with homogeneous isotropic multilayered structures *Phys. Rev.* E **79** 047602

[39] Li C, Meng X K, Liu X, Li F, Fang G Y, Chen H Y and Chan C T 2010 Experimental realization of a circuit-based broadband illusion-optics analogue *Phys. Rev. Lett.* **105** 233906

[40] Zang X F, Li J J, Mao J F and Jiang C 2012 Experimental demonstration of the wave squeezing effect based on inductor-capacitor networks *Appl. Phys. Lett.* **101** 074104

[41] Li J J, Zang X F, Mao J F, Tang M, Zhu Y M and Zhuang S L 2013 Overlapped optics induced perfect coherent effects *Sci. Rep.* **3** 3569